Simple Models of Coastal-Trapped Waves Based on the Shape of the Bottom Topography

L. ZAVALA SANSÓN

Department of Physical Oceanography, CICESE, Ensenada, Mexico

(Manuscript received 11 March 2011, in final form 7 October 2011)

ABSTRACT

Solutions of barotropic coastal-trapped waves in the shallow-water context are discussed for different shapes of the bottom topography. In particular, an infinite family of topographic waves over continental shelves characterized by a shape parameter is considered. The fluid depth is proportional to x^s, where x is the offshore coordinate and s is a real, positive number. The model assumes the rigid-lid approximation and a semi-infinite domain $0 \le x \le \infty$. The wave structure and the dispersion relation depend explicitly on the shape parameter s. Essentially, waves over steeper shelves possess higher frequencies and phase speeds. In addition, the wave frequency is independent of the alongshore wavenumber k, implying a zero group velocity component along the coast. The advantages and limitations of this formulation, as well as some comparisons with other models, are discussed in light of numerical simulations for waves over arbitrary topography within a finite domain. The numerical calculations show that the frequency of the waves present a nondispersive regime at small wavenumbers (observed by several authors), followed by a constant value predicted by the analytical solutions for larger k. It is concluded that these frequencies can be considered as an upper limit reached by barotropic coastal-trapped waves over the infinite family of x^s-bottom profiles, regardless of the horizontal and vertical scales of the system. The modification of the dispersion curves in a stratified ocean is briefly discussed.

1. Introduction

This paper examines the properties of subinertial coastal-trapped waves in the ocean according to simple barotropic models. In the absence of stratification, these oscillations are mainly affected by both the earth's rotation and the shape of the bottom topography. Subinertial topographic waves are also referred to as continental shelf waves, and they travel along the coast with shallow water to the right (left) in the Northern (Southern) Hemisphere. In this sense, the oscillatory motions are trapped or attached to the coast. The existence of these waves is associated with conservation of potential vorticity, and therefore they are sometimes referred to as vorticity waves. In contrast, superinertial oscillations, also called edge waves, are basically gravity waves affected by rotation and topography, which travel in any direction along the coast. Topographic waves have been thoroughly studied in the last 60 yr from the theoretical, observational, numerical, and experimental points of view by a large number of researchers. Important reviews are those by Mysak (1980) and Brink (1991).

Besides the barotropic limit and subinertial frequencies, we focus our attention to free waves (with no external forcing) propagating along a straight boundary. The fluid depth over the coastal topography is assumed as a monotonic function $h(x)$, where x is the offshore coordinate. In general, wave characteristics vary over different bottom topographies. Therefore, there are no universal solutions or general dispersion relations for coastal-trapped waves (Huthnance 1975), because they depend directly on the shape of the shelf. Thus, the bottom topography is often approximated with a well-behaved analytical function, which is typically linear [$h(x) \sim x$; e.g., Reid 1958; Mysak 1968; Cohen et al. 2010] or exponential [$h(x) \sim e^x$; e.g., Buchwald and Adams 1968; Gill and Schumann 1974; Gill 1982], from which the wave properties are derived.

In this paper, we present and discuss a set of wave solutions of the linear shallow-water equations, which depend on the shape of the bottom topography profile.

Corresponding author address: L. Zavala Sansón, Department of Physical Oceanography, CICESE, Carretera Ensenada-Tijuana 3918, 22860, Ensenada, Baja California, Mexico.
E-mail: lzavala@cicese.mx

DOI: 10.1175/JPO-D-11-053.1

Such a profile is assumed as $h(x) \sim x^s$, where s is an arbitrary positive shape parameter that determines the monotonically increasing depth of the continental shelf. The basic procedure and the dynamical fields of the waves were reported in a preliminary study by Zavala Sansón (2010a). The aim here is to point out that the solutions, particularly the wave frequencies, explicitly depend on s. This result provides an easy procedure to estimate the frequency of topographic waves over an infinite family of bottom topography profiles, defined by the shape parameter.

The limitations of this and other formulations are discussed. For instance, the analytical dispersion relation indicates that there is no dependence of the wave frequency on the alongshore wavenumber k, which implies a zero group velocity component along the coast. In contrast, some other formulations (e.g., Cohen et al. 2010; Buchwald and Adams 1968) are characterized by dispersion curves with a maximum frequency at a certain k and hence an energy transport along the coast in both directions. Other cases present a zero group velocity for large k (e.g., Reid 1958; Mysak 1968). The approximate superinertial solutions of Mysak (1968) also present a nearly zero group velocity along the coast at intermediate frequencies and wavenumbers; recently, Ke and Yankovsky (2010) discussed this property for semidiurnal oscillations propagating over wide, gently sloping shelves. We emphasize, however, that the present results are restricted to subinertial waves.

Because the present solutions are obtained for a semi-infinite domain $0 \leq x \leq \infty$ and assume the rigid-lid approximation, we compare the analytical dispersion relation with the corresponding curves calculated by means of the numerical scheme developed by Brink and Chapman (1987) for a finite domain. The simulations allow an independent evaluation of the main assumptions and results of the analytical derivation. In general, it is concluded that the predicted frequencies can be regarded as an upper limit reached by barotropic coastal-trapped waves over the infinite family of bottom profiles defined by the parameter s.

The use of a bottom profile with a shape parameter is justified by considering some realistic bottom configurations, as shown in Fig. 1. Four examples of continental topographies at the eastern Pacific Ocean are presented: two at the Northern Hemisphere, Acapulco (Mexico) and Lincoln City (United States), and two at the Southern Hemisphere, Lima (Peru) and Valparaiso (Chile). At these locations the bottom topography is relatively uniform for several kilometers along the coast. Thus, the profiles are plotted for a transect perpendicular to the coast. The bottom topography profile $h(x) = h_0(\lambda x)^s$ is also plotted (dashed lines), where λ^{-1} is the horizontal length scale of the shelf and h_0 is a depth scale. The shape parameter s is indicated below the curves. Evidently, the bottom profiles are characterized by different values of s. It seems reasonable, therefore, to look for wave solutions beyond the linear or exponential profiles.

Another aim of this study is to call the attention to the relatively simple procedure to derive the solutions. A relevant result is that the offshore structure of the waves is obtained in terms of associated Laguerre polynomials. The linear cases studied by Reid (1958) and Mysak (1968) actually depend on simple Laguerre polynomials. This strongly suggests that the analytical method might be applied in problems with different topographic geometries. In fact, a similar family of solutions was reported recently for barotropic waves trapped around seamounts (Zavala Sansón 2010b).

In section 2, we discuss the family of coastal-trapped waves over the $h(x) \sim x^s$ depth profile. In section 3, we make some comparisons between the obtained analytical frequencies and those calculated by means of numerical simulations. Section 4 briefly addresses the influence of stratification on the dispersion curves. Finally, section 5 includes the discussion and general conclusions.

2. Wave solutions

Consider a semi-infinite Cartesian domain (x, y) in a rotating system where $0 \leq x \leq \infty$ and $-\infty \leq y \leq \infty$. The homogeneous fluid layer is bounded by a straight coast at $x = 0$. The linear shallow-water equations are

$$u_t - fv = -g\eta_x, \tag{1}$$

$$v_t + fu = -g\eta_y, \quad \text{and} \tag{2}$$

$$\eta_t + (hu)_x + (hv)_y = 0, \tag{3}$$

where subindices denote partial derivatives, u and v are the velocity components, η is the free-surface deformation, h is the fluid layer depth, and g is gravity. In nondimensional terms, continuity can be written as $\delta\eta_t + (hu)_x + (hv)_y = 0$, where $\delta = L^2/R_d^2$; here L is a horizontal length scale and $R_d = (gH)^{1/2}/f$ the external radius of deformation, with H being a depth scale (besides, $\eta \sim UfL/g$ and $t \sim 1/f$). The rigid-lid approximation considers length scales much shorter than R_d: that is, $\delta \ll 1$ (e.g., Gill and Schumann 1974). Dropping the first term in (3), the velocity components can be defined in terms of a transport function as

$$u = \frac{1}{h}\psi_y, \quad v = -\frac{1}{h}\psi_x. \tag{4}$$

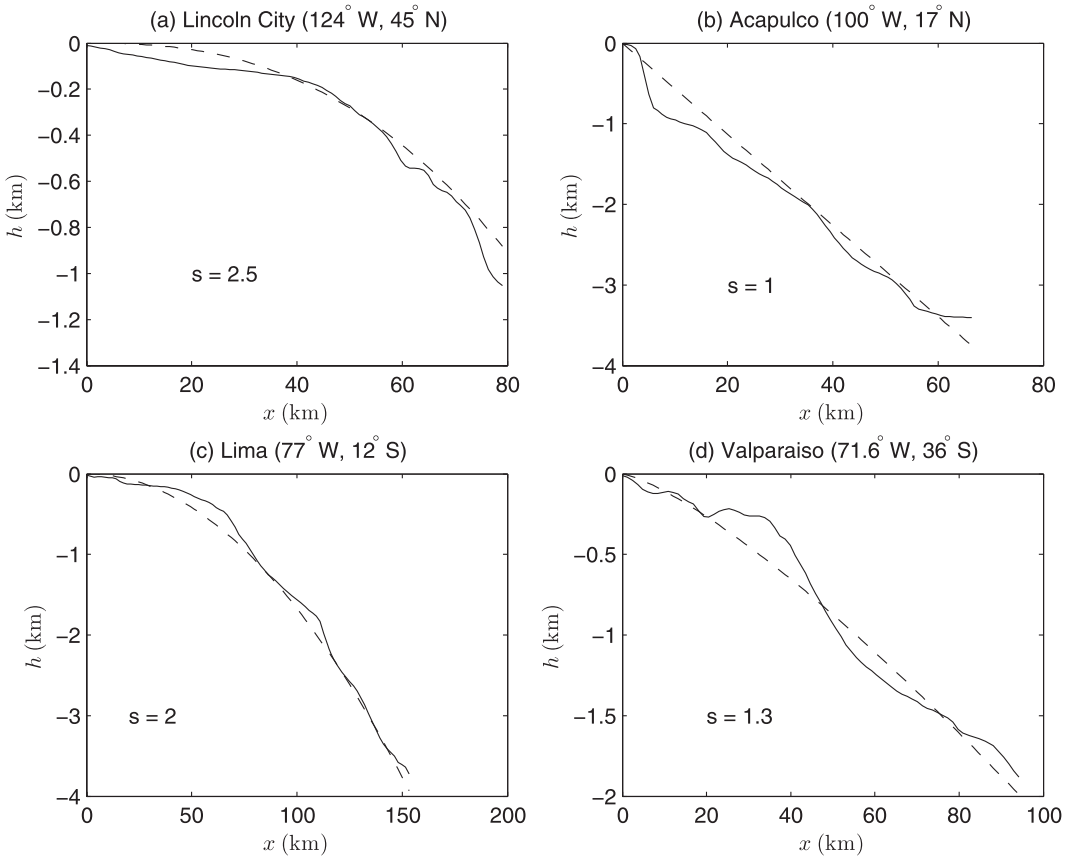

FIG. 1. Profiles of offshore bottom topographies at four locations in the eastern Pacific Ocean. Solid lines are data from 1-minute gridded elevations/bathymetry for the world (ETOPO1; Amante and Eakins 2009). Dashed lines are profile $h = h_0(\lambda x)^s$. The topographic parameters are (a) $h_0 = 294$ m and $\lambda^{-1} = 50$ km; (b) $h_0 = 1995$ m and $\lambda^{-1} = 35$ km; (c) $h_0 = 1248$ m and $\lambda^{-1} = 86$ km; and (d) $h_0 = 835$ m and $\lambda^{-1} = 48$ km. The depth scale h_0 is calculated as the average depth along the transect and the horizontal scale λ^{-1} is such that $h(\lambda^{-1}) = h_0$.

Using (1) and (2), the equation for the z component of the relative vorticity, $v_x - u_y$, is easily derived,

$$(v_x - u_y)_t + f(u_x + v_y) = 0. \tag{5}$$

This expression states that changes of relative vorticity are associated with divergence or convergence of the flow as fluid columns experience changes of depth. This is the basic mechanism of topographic waves. Substituting the derivatives of the velocity components gives an equation for the transport function,

$$\psi_{xxt} + \psi_{yyt} - \frac{h_x}{h}\psi_{xt} + f\frac{h_x}{h}\psi_y = 0. \tag{6}$$

Wave solutions are proposed of the form

$$\psi(x, y, t) = h(x)^{1/2}\phi(x)e^{i(ky+\omega t)}, \tag{7}$$

which yields an equation for ϕ,

$$\phi_{xx} + \left[\frac{1}{2}\left(\frac{h_x}{h}\right)_x - \left(\frac{1}{2}\frac{h_x}{h}\right)^2 + \frac{h_x}{h}\frac{fk}{\omega} - k^2\right]\phi = 0. \tag{8}$$

The solutions must satisfy

$$\phi(x) = 0 \quad \text{at} \quad x = 0 \quad \text{and} \tag{9}$$

$$\phi(x) \to 0 \quad \text{as} \quad x \to \infty. \tag{10}$$

As outlined in the first section, we consider the depth profile as an arbitrary power of x,

$$h(x) = h_0(\lambda x)^s \Rightarrow \frac{h_x}{h} = \frac{s}{x}, \tag{11}$$

where the arbitrary parameter $s > 0$ measures the shape of the shelf and h_0 and λ^{-1} are the vertical and horizontal scales, respectively. Evidently, larger s values mean steeper topographies for $x > \lambda^{-1}$. Figure 2 shows some examples for different values of this parameter. The

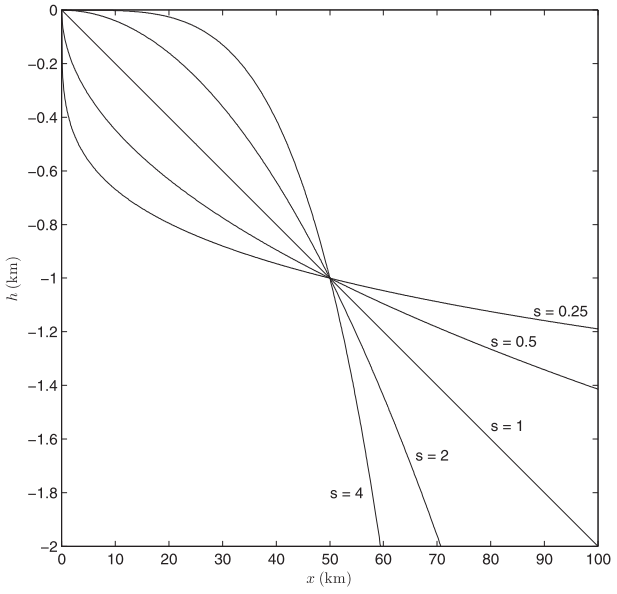

FIG. 2. Depth profiles over continental shelves of the form $h = h_0(\lambda x)^s$ for $s = 0.25, 0.5, 1, 2$, and 4. The topographic parameters are $h_0 = 1000$ m and $\lambda^{-1} = 50$ km.

advantage of this formulation is to find the wave properties as a function of the topography shape. Substituting (11) in (8), the following expression is obtained:

$$\phi_{xx} + \left[-\left(\frac{s}{2} + \frac{s^2}{4}\right)\frac{1}{x^2} + \frac{fks}{\omega}\frac{1}{x} - k^2\right]\phi = 0. \quad (12)$$

Applying the change of variable,

$$\rho = 2kx, \quad \chi(\rho) = \phi(x), \quad (13)$$

yields

$$\chi_{\rho\rho} + \left[-\left(\frac{s}{2} + \frac{s^2}{4}\right)\frac{1}{\rho^2} + \frac{fs}{2\omega}\frac{1}{\rho} - \frac{1}{4}\right]\chi = 0. \quad (14)$$

The solution is obtained in terms of the associated Laguerre polynomials with the following form (see Arfken 1970, p. 620):

$$\chi(\rho) = e^{-\rho/2}\rho^{(j+1)/2}L_p^j(\rho), \quad (15)$$

where the indices j and p are defined by the following relationships:

$$\frac{j^2 - 1}{4} = \frac{s}{2} + \frac{s^2}{4}, \quad j > -1 \in \mathbb{R} \quad \text{and} \quad (16)$$

$$\frac{2p + j + 1}{2} = \frac{sf}{2\omega} \quad p \geq 0 \in \mathbb{Z}. \quad (17)$$

The solutions of the first equation are $j = \pm(s + 1)$. In general, $j > -1$ is a real number and therefore there can only be solutions for arbitrary $s > 0$ for the positive root $j = s + 1$. Index $p \geq 0$ is an integer. The dispersion relation is derived from expression (17),

$$\frac{\omega}{f} = \frac{s}{2(p + 1) + s}. \quad (18)$$

Note that all waves are subinertial over a shelf with arbitrary s and the highest frequency corresponds to the wave with $p = 0$.

To find the complete solutions, we note first that

$$\phi(x) = Ae^{-kx}(2kx)^{(s+2)/2}L_p^{s+1}(2kx), \quad (19)$$

where A is an arbitrary constant with appropriate units. With this expression, the conditions (9) and (10) are satisfied. When substituted in (7), the full solution for the transport function is

$$\psi(x, y, t) = \psi_0\left(\frac{\lambda}{2k}\right)^{s/2}e^{-kx}(2kx)^{s+1}L_p^{s+1}(2kx)e^{i(ky+\omega t)}, \quad (20)$$

where $\psi_0 = Ah_0^{1/2}$ is the arbitrary amplitude.

The horizontal velocity components are calculated by means of expression (4) and taking the real parts,

$$u = -U_0kxe^{-kx}L_p^{s+1}(2kx)\sin(ky + \omega t) \quad \text{and} \quad (21)$$

$$v = -U_0e^{-kx}[(p + s + 1)L_p^s(2kx) - kxL_p^{s+1}(2kx)]\cos(ky + \omega t), \quad (22)$$

where the (arbitrary) velocity amplitude is defined as $U_0 = (\psi_0/h_0)[(2k)^{s/2+1}/\lambda^{s/2}]$. To obtain v, the x derivative of the transport function was calculated by using the following recurrence relation of the associated Laguerre polynomials (Abramowitz and Stegun 1972):

$$\rho[L_p^{s+1}(\rho)]_\rho = pL_p^{s+1}(\rho) - (p + k)L_{p-1}^{s+1}(\rho). \quad (23)$$

To write the polynomials with indices within the range of permitted values, an additional recurrence relation was also used,

$$L_{p-1}^{s+1}(\rho) = L_p^{s+1}(\rho) - (p + s + 1)L_p^s(\rho). \quad (24)$$

The structure of the waves for different values of the shape parameter s is thoroughly described in Zavala Sansón (2010a). Essentially, the oscillations are a set of positive and negative relative vorticity patches arranged along the coast, traveling in the negative y direction: that

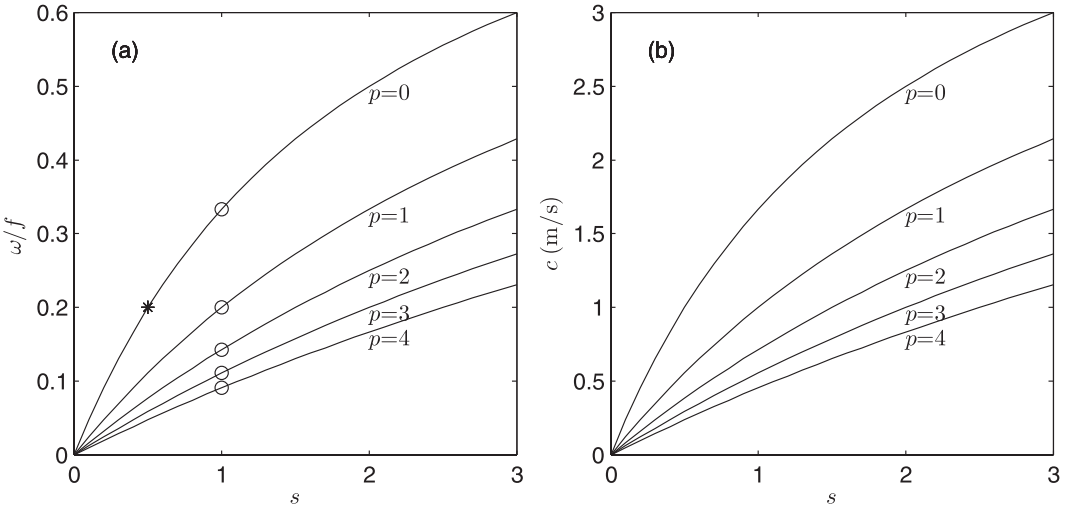

FIG. 3. (a) Wave frequency as a function of the shape parameter for modes $p = 0, \ldots, 4$, given by expression (18). The circles indicate the frequency for the linear shelf $s = 1$ predicted by Reid (1958). The star indicates the frequency of the gravest mode over a shelf with $s = ½$ calculated by Huthnance (1978). (b) Corresponding phase speeds (25) for the modes of a wave with $k = 1/50\,\mathrm{km}^{-1}$.

is, with shallow water to the right. The patches have maxima and minima at the coast, and they rapidly decay offshore. An important point to notice is that the waves are trapped within a distance of order k^{-1}, (i.e., determined by their own size along the boundary) because of the factor e^{-kx}. The offshore structure of the waves is characterized by an oscillatory vorticity and velocity profile with strongly decreasing amplitude for large offshore distances ($u, v \to 0$ for $x \gg \lambda^{-1}$). Index p indicates the number of zero crossings of the offshore vorticity profile. Thus, p is a natural measure of the offshore wavenumber.

3. Wave properties

The dispersion relation depends directly on the shape parameter s and the offshore mode p, as expression (18) indicates. Wave frequencies as a function of the shape parameter for the first five p modes are presented in Fig. 3a. These curves show that low s values imply lower frequencies, or waves with higher frequencies are developed over steeper slopes. Also, the gravest mode $p = 0$ possesses the higher frequency over any topography. The predicted values for linear slopes, $s = 1$, calculated by Reid (1958) are shown with a circle (the linear slope is further discussed below). On the other hand, the star over the curve of the gravest mode $p = 0$ indicates the frequency of a wave over a topography proportional to $x^{1/2}$. This value was analytically calculated by Huthnance (1978) as $\omega/f = [-2 + (9 + 5Sk)^{1/2}]/5$, with S a stratification parameter; for the barotropic case ($S = 0$), the present result is recovered, $\omega/f = 1/5$.

The waves are dispersive with phase speed

$$c = -\frac{\omega}{k} = -\frac{fs}{k(2p + s + 2)}, \tag{25}$$

so larger waves (smaller k) travel faster. For a given wave (fixed k), the phase speed as a function of the shape parameter has the same behavior as the frequency curves, as shown in Fig. 3b. In other words, waves over steep shelves travel faster than waves over weaker slopes.

The simple character of the dispersion relation demands a deeper investigation on the restrictions imposed in the present derivation (e.g., the group velocity $\partial\omega/\partial k$ is null). One of those assumptions is the semi-infinite plane $0 \le x \le \infty$, which implies that the depth field increases indefinitely in the offshore direction. Thus, an important question is whether the solutions change significantly when a flat-bottom abyssal ocean is included. To answer this point, we have performed numerical simulations with the code written by Brink and Chapman (1987), in order to find the frequencies associated with barotropic waves over arbitrary topography. Basically, the numerical scheme reduces the dependent variables of the linear shallow-water equations into a two-dimensional eigenvalue problem for pairs (ω, k); by fixing a given k, the code searches for resonant frequencies ω by using an iterative process. The bottom profile $h(x) = h_0(\lambda x)^s$ is prescribed up to a maximum depth of $2h_0$ (for the linear profile such a distance is $2\lambda^{-1}$). The numerical domain is extended an additional distance of typically $2\lambda^{-1}$, along which the depth field maintains the same value. Thus, the offshore coordinate is defined as $0 \le x \le 4\lambda^{-1}$.

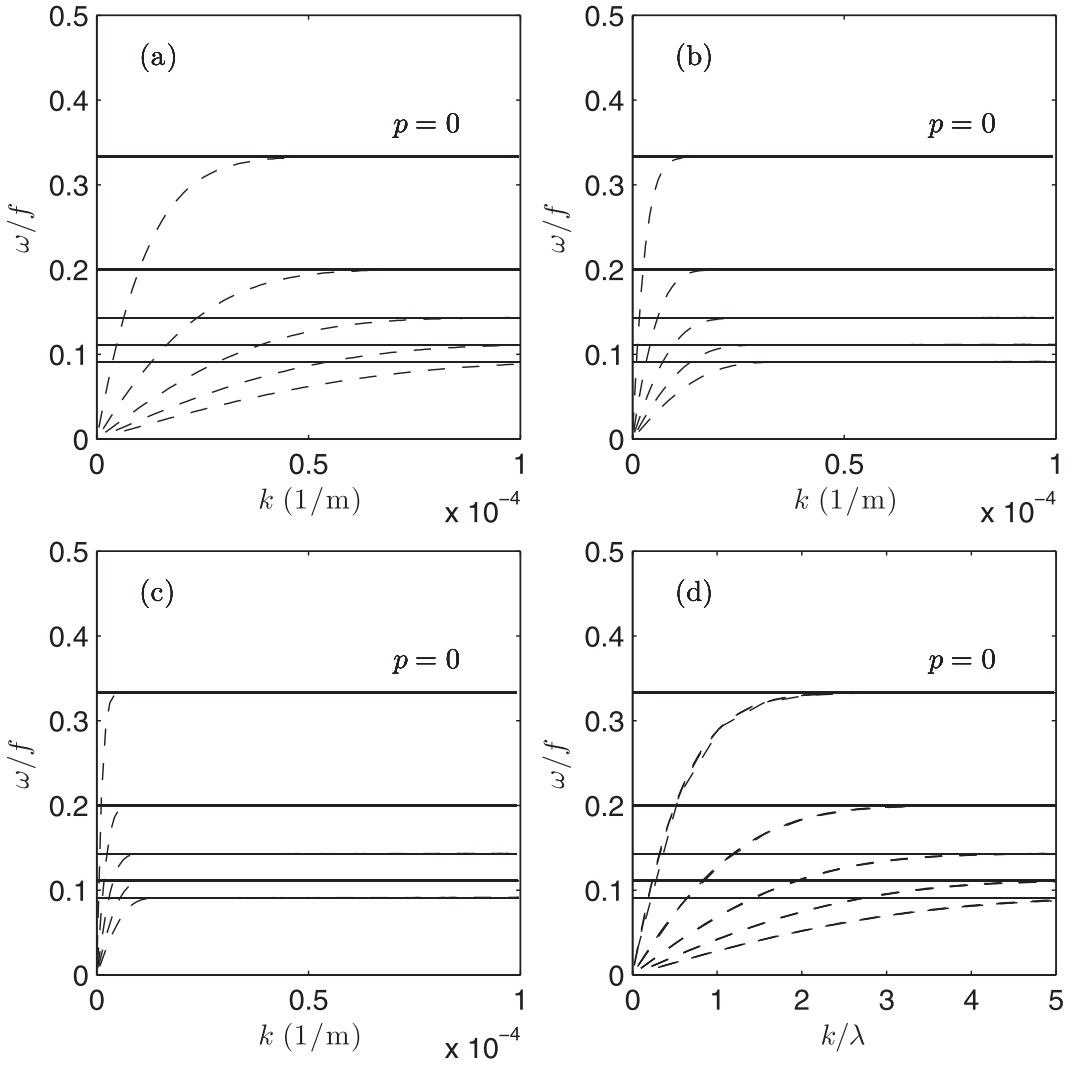

FIG. 4. Dispersion relation for modes $p = 0, \ldots, 4$ calculated for linear topographies, $s = 1$, and topographic parameters (a) $\lambda^{-1} = 50$ km and $h_0 = 200$ m, (b) $\lambda^{-1} = 200$ km and $h_0 = 2000$ m, and (c) $\lambda^{-1} = 500$ km and $h_0 = 2000$ m. Solid lines indicate the present model given by (18). Dashed lines indicate the numerically calculated dispersion curves. (d) Dispersion relation for the three previous cases, but now as a function of k/λ. The numerical curves (dashed) are indistinguishable.

Using this configuration, several simulations were performed for different topographic parameters (h_0, λ^{-1}, and s). Some other numerical parameters are described in the appendix.

Figures 4a–c present the behavior of the dispersion relations over three linear topographies ($s = 1$) with very different vertical and horizontal scales. Note that the k axis has dimensions. In all cases, the dispersion relation presents a linear behavior for very long waves (i.e., they are nondispersive), until reaching the constant limit predicted by the present solutions (1/3, 1/5, 1/7, ...). This behavior is found for several different combinations of the topographic parameters. Thus, a first conclusion is that the solutions do not change significantly in a finite domain and a flat-bottom abyssal ocean, except for small k. This is not surprising because the solutions are based on the rigid-lid approximation, which demands length waves shorter than the deformation radius. Note that the frequencies of all modes reach the analytical values at a smaller k for wider topographies (larger λ^{-1}). In other words, the range of waves that reach the analytical frequencies is larger for wider shelves. There is another observation: the dispersion relation (18) indicates a set of specific frequency values for a given parameter s, regardless of h_0 and λ^{-1}. This property is verified by plotting the dispersion relation in the adequate nondimensional

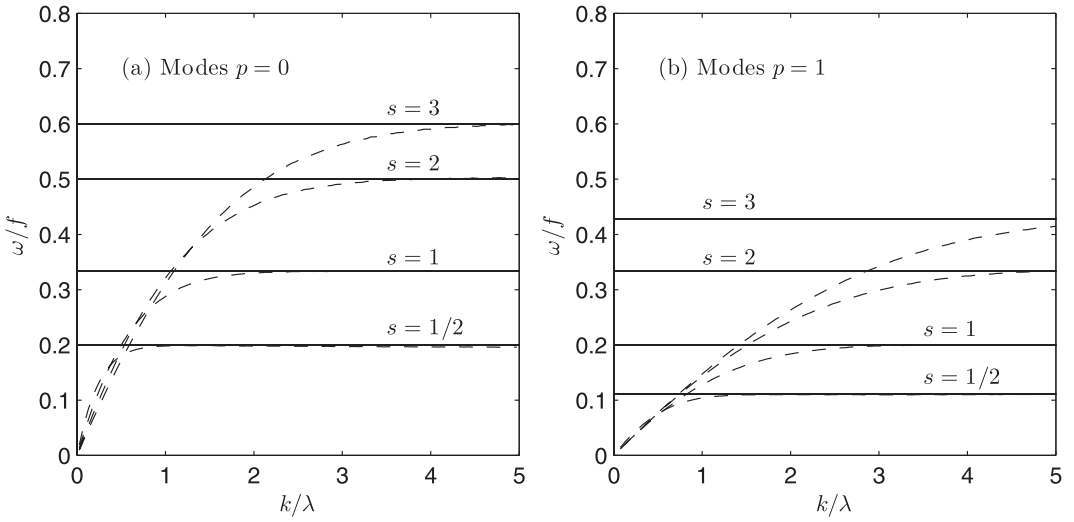

FIG. 5. Dispersion relation for modes (a) $p = 0$ and (b) $p = 1$, calculated for topographies with shape parameter $s =$ 0.5, 1, 2, and 3. Solid lines indicate the present model given by (18). Dashed lines indicate the numerically calculated dispersion curves.

units, as shown in Fig. 4d. Here, the curves of Figs. 4a–c are plotted together in terms of k/λ. Evidently, the frequencies associated to each mode are indistinguishable.

We can now analyze numerically some cases for different shape parameters. Figure 5 presents the dispersion curves of the two first modes ($p = 0$ and 1) over bottom profiles with $s = ½, 1, 2$, and 3. Recall that higher s values imply higher frequencies. The simulations indicate that the predicted frequencies for both modes are reached at smaller k for smaller s. For instance, for $s = ½$ the wave mode $p = 0$ reaches the predicted value, ⅕, for wavelengths shorter than the width of the shelf ($k^{-1} < \lambda^{-1}$). In contrast, for $s = 3$ only those waves with $4k^{-1} < \lambda^{-1}$ present the predicted value, ⅗. A similar situation occurs for mode $p = 1$. The simulations were performed with $h_0 = 200$ m and $\lambda^{-1} = 50$ km. However, recall that the form of the ω/f versus k/λ curves is independent of these values.

4. Some effects of stratification

We have seen that the theoretical frequencies obtained for the rigid-lid waves with the dispersion relation [(18)] are an upper limit for barotropic waves over an arbitrary bottom profile x^s (for x bounded or unbounded). Because stratification is of fundamental importance in the ocean, it is useful to explore the modification of the dispersion curves in the presence of this additional effect. Here, we discuss the dispersion relation in a stratified fluid obtained by means of the numerical solver for baroclinic waves written by Brink and Chapman (1987). We shall limit the discussion only to a few cases with uniform stratification. It is anticipated that the frequency of the waves is increased in a stratified ocean, as has been shown in other studies (e.g., Brink 1982; Huthnance 1978). We analyze two bottom topographies with $s = 1$ and 2. The numerical domain and parameters are equivalent to those used for the barotropic case (see the appendix), except that now we prescribed a uniform Brunt–Väisälä frequency N^2 over the whole fluid depth.

Figure 6a shows the dispersion relations for the zeroth mode ($p = 0$) over a linear topography ($s = 1$) for four different values of N^2, ranging from 10^{-6} s^{-2} (typical of the abyssal ocean) to 10^{-4} s^{-2} (typical of the pycnocline at the upper ocean). The analytical value, ⅓, is represented by the horizontal line. It can be observed that the nondispersive regime for small k is very similar in all cases. As the frequencies approach the barotropic limit, the curves bend almost horizontally. The waves with weak and moderate stratification (two lowest curves) are very close each other and remain relatively close to the barotropic frequency (maximum difference of ≈1%). Thus, for moderate N^2 the dispersion curves are very similar to the barotropic limit over the linear topography. For larger stratifications, the curves depart about 24%. Note that there is a weak tendency to decay for larger k.

Figure 6b shows the corresponding curves of the same mode over a quadratic profile, $s = 2$. The barotropic limit is ½. Weak stratifications remain very close again (two lower curves), but now they present a departure from the horizontal line of about 10% at $k/\lambda \approx 2.8$. Strong stratifications (two upper curves) imply strong deviations from the barotropic limit (more than 40% for

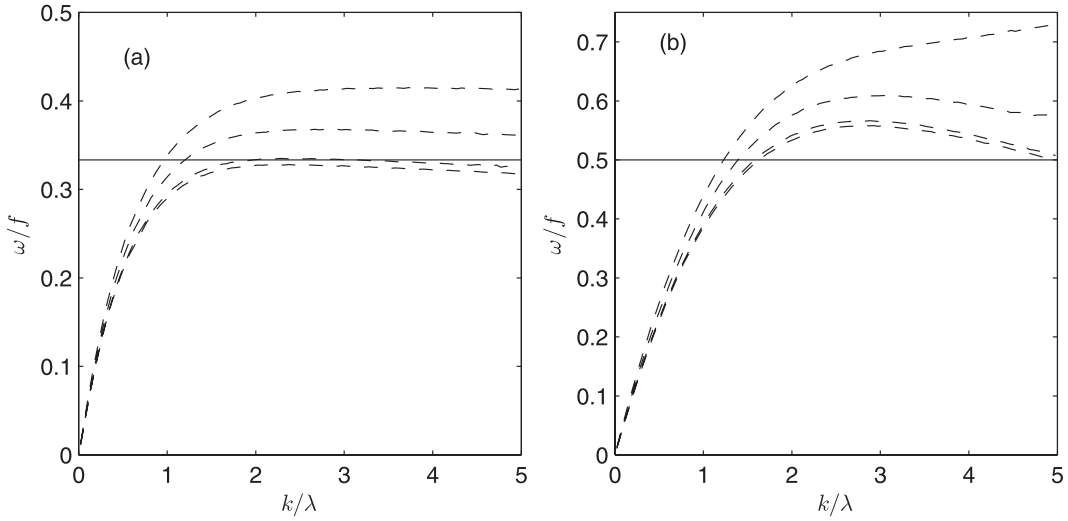

FIG. 6. (a) Numerically calculated dispersion curves (dashed lines) for mode $p = 0$ over a linear topography $s = 1$, in the presence of stratification: $N^2 = 10^{-6}$, 10^{-5}, 5×10^{-5}, and 10^{-4} s^{-2} for curves in ascending order. The horizontal line is the barotropic limit 1/3. The topographic parameters are $h_0 = 200$ m and $\lambda^{-1} = 50$ km. (b) As in (a), but for a quadratic topography $s = 2$. The horizontal line is the barotropic limit ½.

the highest stratification). The decaying tendency of the lowest three curves is evident.

5. Discussion

Solutions of barotropic, rigid-lid topographic waves over a continental shelf with different depth profiles have been presented. The waves are characterized by subinertial frequencies and by their propagation along the coast with shallow water to the right (left) in the Northern (Southern) Hemisphere. The wave solutions are based on the shape of the bottom profile proportional to x^s, where s is a real, arbitrary positive number. These solutions allow the description of coastal-trapped waves over an infinite set of continental shelves defined as powers of the offshore coordinate. The waves are trapped in the sense that they rapidly decay in the offshore direction as e^{-x}. A remarkable characteristic of the solutions is that the dispersion relation is a very simple expression, (18), given in terms of the shape parameter s and the offshore wavenumber index p (=0, 1, 2, 3, ...). This allows an easy estimation of the wave frequencies and phase speeds depending on the shape of the bottom profile (Fig. 3).

An important assumption is the use of a semi-infinite domain over which the x^s topography is defined. To investigate the consequences of this approach, we performed numerical simulations with the code of Brink and Chapman (1987) in order to find the corresponding wave frequencies in a finite domain. In the simulations, the bottom profile $h = h_0(\lambda x)^s$ is defined up to $x = 2\lambda^{-1}$ and beyond that point the bottom becomes flat with $h = 2h_0$. The numerical results have showed that the waves present a nondispersive regime for very long waves (small k; Mysak 1980), and then reach the frequency given by (18) for k larger than a few times λ (Figs. 4, 5). This is in agreement with the rigid-lid approximation, which assumes that the waves have to be shorter than the deformation radius. Besides, the numerical simulations showed that the dispersion relations ω/f versus k/λ are identical (for a given s), regardless of the depth scale and the width of the shelf. This was indeed anticipated from the analytical dispersion relation, which indicates that the frequency of the different modes does not depend on the topographic parameters h_0 and λ but only on the shape parameter s. Thus, the analytical results obtained for a semi-infinite domain can be applied for a finite-depth topography for k/λ sufficiently large (depending on s). A fair conclusion is that the frequencies predicted in the present solutions can be regarded as the upper limits reached by barotropic wave modes over the infinite family of the x^s-bottom profiles.

The wave frequencies predicted in (18) can be directly compared with respect to some other formulations. One of the earliest studies in topographic waves was reported by Reid (1958), who examined the case of a linear bottom profile in a semi-infinite domain. The frequencies showed a nondispersive regime for small k, after which they rapidly tend to the values given by (18) for $s = 1$. An additional complication arises when considering a shelf of finite width, as shown by Mysak (1968). In that study, the wave solutions over the linear shelf were coupled with an external solution outside, where the depth was

considered constant (as in our numerical simulations). As a result, the dispersion curves described by Reid (1958) are modified for small k (see Fig. 5 in Mysak 1980), but the frequency limits given by (18) are obtained for large k again.

The dispersion relation over a linear topography can present a different behavior by introducing very subtle variations in the bottom profile. Such is the case of a linear topography, but now with a nonzero depth at $x = 0$. In the formulation of Cohen et al. (2010), the authors considered a fluid depth of the form $h(x) = H_0 + H'x$, where H_0 is a nonzero depth at the coast and H' the slope. The results were oriented to explain observations in laboratory experiments. The wave modes are given in terms of the zeros of the Airy function. The dispersion curves have a maximum frequency for each mode, after which the frequency slowly diminishes for larger wavenumbers [see their Eq. (11) and their Fig. 3].

Another well-known depth profile is the exponential function $h(x) = H_0e^{2b\lambda x}$, where H_0 is the depth at the coast and b is a real, positive number. This profile was used by Buchwald and Adams (1968) and by Gill and Schumann (1974), among others. The exponential topography strongly simplifies the offshore structure of the waves to harmonic functions: for instance, $\sin(lx)$, where l is the offshore wavenumber. The model of Buchwald and Adams (1968) considers a finite exponential profile and assumes a flat bottom beyond a given shelf width. The case of a semi-inifinite plane is presented in the textbook by Gill (1982, 409–410). The dispersion curves for the exponential topography are characterized by a maximum frequency for each mode and a rapid decay for large k.

Considering the shape of the dispersion relations described in last two paragraphs, the independence of the wave frequency with wavenumber in (18) deserves some additional comments. The general analysis of Huthnance (1975) predicts a nondispersive regime for small k and a decaying frequency for large k, which is verified in the models of Buchwald and Adams (1968) and Cohen et al. (2010), among others. As a consequence, waves in these models transport energy along the coast in both directions, because the alongshore group velocity changes sign at a maximum frequency. A necessary condition, however, is that h_x/h is bounded for all x. This is not the case in the present formulation at $x = 0$ ($h_x/h = s/x$), so this hypothesis does not hold. As a consequence, the zero group velocity found here does not contradict Huthnance's theorem. A similar situation explains the zero group velocity for large k in the models of Reid (1958) and Mysak (1968).

It must be mentioned that the precise shape of the dispersion curves in most of previous models might be very sensitive to the topographic parameters: for example, the depth at the coast H_0. In addition, some of them consider wave solutions over a finite shelf, coupled with an external solution outside, where the depth was considered constant, as mentioned above for the linear and exponential profiles. This procedure implies the solution of transcendental equations in order to match the internal and external solutions, which difficults the application of the resulting dispersion relations. In contrast, for the x^s profiles the maximum frequencies can be easily estimated as a function of the shape of the topography given by s, without assuming necessarily a linear or an exponential shape. Other topographic parameters do not alter the dispersion curves. An important limitation is that the theory cannot be applied for waves longer than the width of the coastal topography or used to explain energy transport along the coast. Because of these advantages and disadvantages in all formulations, caution must be taken when a model is invoked to explain or predict wave frequencies in oceanographic observations, where usually the errors of the measurements are rather large. Summarizing, the behavior of topographic waves might strongly differ depending on the model considered. In other words, as discussed by Huthnance (1975), there is no universal dispersion relation for waves over arbitrary topography.

As a final remark, it must be recalled that another important factor in oceanic conditions is the stratification. According to the analysis by Huthnance (1978), a uniform stratification over a sloping bottom tends to increase the frequency of the waves (see, e.g., his Fig. 8). Such an increase slightly surpasses the limit values derived here for weak stratification over a linear topography, as shown in the numerical simulations in previous section. The difference becomes more important over a quadratic profile, especially for high N^2 values. These results provide a general idea on the effects of uniform stratification. Nevertheless, additional work is required to discuss more general cases: that is, nonuniform stratification and the influence of different topographic parameters.

Acknowledgments. The author gratefully acknowledges the comments of J. M. López Mariscal and the fruitful remarks and recommendations of two anonymous reviewers.

APPENDIX

Numerical Parameters

The numerical dispersion relations for barotropic waves over arbitrary topography were calculated by using the code BTCSW.FOR of Brink and Chapman (1987). Equivalent values are used in the code BIGLOAD4.FOR

for baroclinic waves (for the stratified case the numerical code demands a nonzero depth at the coast; in all cases we have used 10 m at $x = 0$). Using their notation for the input files, some relevant numerical parameters are the following:

The number of grid points in the x direction is NN = XMAX/dx, where XMAX = $4\lambda^{-1}$ is the distance (km) from $x = 0$ to the offshore boundary of the grid and dx = 500 m is the resolution in all cases.

To find the resonant frequencies, up to NITM = 50 iterations were prescribed, with a fractional accuracy EPS = 0.001 and a fractional step size for the initial search DEL = 0.001.

The boundary conditions were prescribed as IDD3 = 2 and IDD4 = 1 (exponentially decaying condition at x = XMAX and zero normal flow at the boundary, respectively).

The number of pairs (ω, k) was fixed at NCALM = 100 in all simulations. The wavenumbers are defined as k = [RLF + (n − 1)DRL] × 10^{-5} m^{-1}, where n ranges from 1 to NCALM. To find the resonant modes, the initial k (n = 1) was chosen by varying RLF within a range of 0.1–7. The increment was fixed at DRL = 1 in all cases.

REFERENCES

Abramowitz, M., and I. A. Stegun, 1972: *Handbook of Mathematical Functions*. National Bureau of Standards, 1046 pp.

Amante, C., and B. W. Eakins, 2009: Etopo1 1 Arc-Minute Global Relief Model: Procedures, data sources and analysis. NOAA Tech. Memo. NESDIS NGDC-24, 19 pp.

Arfken, G., 1970: *Mathematical Methods for Physicists*. Academic Press, 815 pp.

Brink, K. H., 1982: A comparison of long coastal trapped wave theory with observations off Peru. *J. Phys. Oceanogr.,* **12,** 897–913.

——, 1991: Coastal-trapped waves and wind-driven currents over the continental shelf. *Annu. Rev. Fluid Mech.,* **23,** 389–412.

——, and D. C. Chapman, 1987: Programs for computing properties of coastal-trapped waves and wind-driven motions over the continental shelf and slope. 2nd ed. Woods Hole Oceanographic Institution Tech. Rep. WHOI-87-24, 119 pp.

Buchwald, V. T., and J. K. Adams, 1968: The propagation of continental shelf waves. *Proc. Roy. Soc.,* **305A,** 235–250.

Cohen, Y., N. Paldor, and J. Sommeria, 2010: Laboratory experiments and a non-harmonic theory for topographic rossby waves over a linearly sloping bottom on the f-plane. *J. Fluid Mech.,* **645,** 479–496.

Gill, A. E., 1982: *Atmosphere–Ocean Dynamics*. Academic Press, 662 pp.

——, and E. H. Schumann, 1974: The generation of long shelf waves by the wind. *J. Phys. Oceanogr.,* **4,** 83–90.

Huthnance, J. M., 1975: On trapped waves over a continental shelf. *J. Fluid Mech.,* **69,** 689–704.

——, 1978: On coastal trapped waves: Analysis and numerical calculation by inverse iteration. *J. Phys. Oceanogr.,* **8,** 74–92.

Ke, Z., and A. E. Yankovsky, 2010: The hybrid Kelvin–edge wave and its role in tidal dynamics. *J. Phys. Oceanogr.,* **40,** 2757–2767.

Mysak, L. A., 1968: Edgewaves on a gently sloping contiental shelf of finite width. *J. Mar. Res.,* **26,** 24–33.

——, 1980: Topographically trapped waves. *Annu. Rev. Fluid Mech.,* **12,** 45–76.

Reid, R. O., 1958: Effects of coriolis force on edge waves. (i) Investigation of the normal modes. *J. Mar. Res.,* **16,** 109–144.

Zavala Sansón, L., 2010a: Solutions of continental shelf waves based on the shape of the bottom topography. *The Ocean, The Wine and The Valley: The Lives of Antoine Badan,* E. Pavía, J. Sheinbaum, and J. Candela, Eds., Centro de Investigación Científica y de Educación Superior de Ensenada (CICESE), 103–130.

——, 2010b: Solutions of barotropic trapped waves around seamounts. *J. Fluid Mech.,* **661,** 32–44.